ACS APPLIED MATERIALS & INTERFACES

Research Article

www.acsami.org

Enhanced Sensitivity and Stability of Room-Temperature NH_3 Sensors Using Core–Shell CeO_2 Nanoparticles@Cross-linked PANI with p–n Heterojunctions

Lingling Wang, Hui Huang, Songhua Xiao, Daoping Cai, Yuan Liu, Bin Liu, Dandan Wang, Chenxia Wang, Han Li, Yanrong Wang, Qiuhong Li, and Taihong Wang*

Pen-Tung Sah Institute of Micro-Nano Science and Technology, Xiamen University, Xiamen, China

Supporting Information

ABSTRACT: We report a room-temperature NH_3 gas sensor with high response and great long-term stability, including CeO_2 NPs conformally coated by cross-linked PANI hydrogel. Such core–shell nanocomposites were prepared by in situ polymerization with different weight ratios of CeO_2 NPs and aniline. At room temperature, the nanohybrids showed enhanced response (6.5 to 50 ppm of NH_3), which could be attributed to p–n junctions formed by the intimate contact between these two materials. Moreover, the stability was discussed in terms of phytic acid working as a gelator, which helped the PANI sheath accommodate itself and enhance the mechanical strength and chemical stability of the sensors by avoiding "swelling effect" in high relative humidity. The sensors maintained its sensing characteristic (response of ca. 6.5 to 50 ppm of NH_3) in 15 days. Herein, the obtained results could help to accelerate the development of ammonia gas sensor.

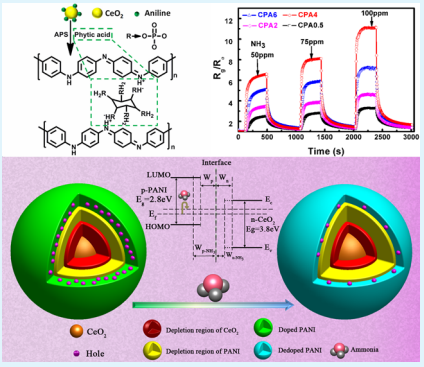

KEYWORDS: *CeO_2 NPs, PANI hydrogel, NH_3 sensor, p–n junction, phytic acid, core–shell*

1. INTRODUCTION

Among the toxic gases of interest, ammonia is a prominent instance for its wide usage in industrial coolant and IC manufacturing.[1] In addition, ammonia pollutions through three major origins including aerosols from atmospheric depositions, ammonification by nitrogen cycle and combustion of chemical materials will cause dramatic environmental problems in daily life.[2] Therefore, there is a practical meaning to fabricate sensitive, stable, and low-cost sensors ensuring NH_3 monitor working at room temperature for the prosperous applications of environmental surveillance. Although inexpensive and stable metal oxide (MOX)-based ammonia sensors have already been extensively researched and manufactured, obvious drawbacks such as high working temperature or low selectivity make it unsuitable for monitoring ambient conditions.[3−5]

Meanwhile, the low operating temperature and high response were observed from the conducting polymer (CP) NH_3 sensors, but their intrinsic unstability restricts their real applications.[6−10] Thus, further work should be performed to improve the long-term performance of organic polymer before real applications. Recently, CP hydrogel has already been demonstrated in energy storage material[11,12] and biosensors[13,14] because of its porous structure, high electrical conductivity, large mechanical strength and great long-term stability. The cross-linked PANI hydrogel could be made using additive "gelators" working as a nanoscaffold to enhance the polymer framework. It has been reported that pure PANI hydrogel showed superior cycling performance in supercapacitors by avoiding swelling and shrinking during intensive charging and discharging process.[11] It is expected that using PANI hydrogel can also function as NH_3 sensors with high sensitivity, fast response, together with great stability especially.

Furthermore, to possess the advantages of not only highly stable inorganic materials such as MOX, noble metal, and low-dimensional carbon material but also organic CP with great synthetic versatility and low operating temperature, different kinds of active materials based on organic–inorganic hybrids have been extensively fabricated such as one-dimensional coaxial nanowires of SnO_2/PPY, CNT/PANI and MoS_2/PANI,[15−18] two-dimensional nanosheets including reduced graphite oxide/PANI and graphite oxide/PANI,[19,20] and three-dimensional hierarchical nanostructures, e.g., iron oxide/PEDOT:PSS, PE-*co*-GMA/PANI, Pd/PANI, and β-$AgVO_3$/PANI.[21−24] In order to synthesis these hybrid materials, layer-by-layer self-assembly,[25] vapor-deposition,[15,26] electrodeposition,[27] and electrospinning route[28,29] have been used for their higher adhesive strength and ultrathin film deposited on different substrates. Recently, in situ polymerization in the presence of inorganic materials has caught much attention for its low cost.[21,30,31] What's more, even if conducting polymers are generally insoluble and show low hydrophilicity, CP hydrogel can be prepared in aqueous media with cross-linker by in situ polymerization.[12] In this work, we report a facile in situ polymerization method to synthesis CeO_2

Received: June 3, 2014
Accepted: July 18, 2014
Published: July 18, 2014

   dx.doi.org/10.1021/am503286h | ACS Appl. Mater. Interfaces 2014, 6, 14131−14140

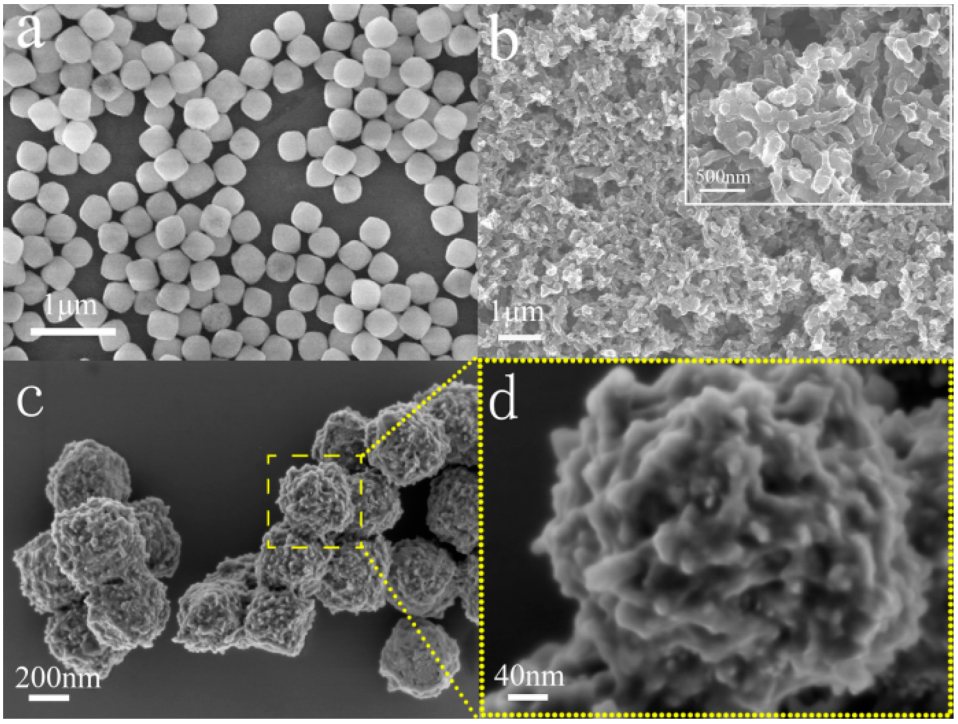

Figure 1. (a, b) SEM images of CeO_2 nanoparticles and pure PANI hydrogel cross-linked by phytic acid. (c, d) SEM images of core−shell structure of CPA4 in both low and high magnification.

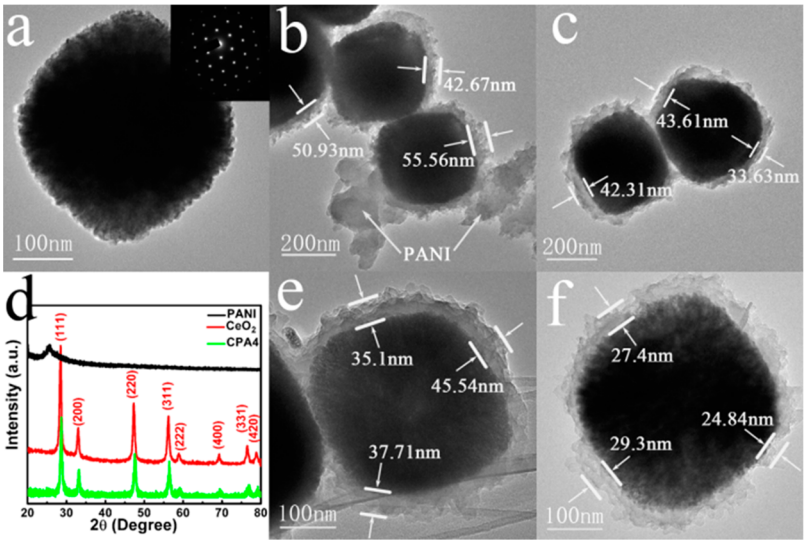

Figure 2. (a) Typical TEM image of CeO_2 nanoparticle (SAED pattern in inset). (b,c, e, f) TEM images showing different coating thicknesses of PANI on the CeO_2 nanoparticle of CPA0.5, CPA2, CPA4, and CPA6. (d) XRD patterns of pure PANI, CeO_2, and CeO_2@PANI hybrids.

NP@PANI hydrogel nanohybrids by using phytic acid worked as gelator and dopant simultaneously. The n-type core CeO_2 NPs, together with the conformally coated p-type PANI hydrogel shell, formed a resistive p−n junction that could help the realization of highly sensitive, fast-response NH_3 sensor with great long-term stability at room temperature. The sensing response was not changed after 15 days, in contrast to a 40% degradation of the sensing response after 4 days in ref 10.

2. EXPERIMENTAL SECTION

2.1. Materials. Aniline (purchased, analytical purity, Sinopharm Chemical Reagent Co., Ltd.) was distilled under reduced pressure before use. Ammonium peroxydisulfate (APS, $(NH_4)_2S_2O_8$), ammonium hydroxide (25%), phytic acid (50%, wt/wt in water, aladdin), ceric ammonium nitrate, polyvinylpyrrolidone (PVP K30), and ethyl alcohol were all of analytical purity and used without further purification.

2.2. Synthesis of CeO_2 Nanoparticles. First, 0.54 g (1 mmol) of ceric ammonium nitrate was dissolved in 3 mL of deionized (DI) water, and then 3 mL of ethyl alcohol, 0.315 g of PVP, and 0.07 mL of ammonium hydroxide were successively added into the solution. The solution was stirred for 10 min and then poured into a 20 mL Teflon-lined autoclave heated to 200 °C for 12 h. The reacted precipitate was cleaned with DI water and ethanol several times and then dried at 60 °C for 12 h. The dried CeO_2 nanoparticles were thermally treated at 500 °C for 3 h in air, and the CeO_2 nanoparticles were then obtained.

2.3. Synthesis of CeO_2 NP@PANI Hybrid. In a typical synthesis, 0.0715 g (0.3125 mmol) of APS was dissolved in 0.5 mL of DI water (solution A). Solution B was prepared by mixing 0.690 mL (1 mmol) of phytic acid, 0.069 mL (0.75 mmol) of aniline, 0.27 g of CeO_2 nanoparticles and 4.5 mL of DI water. The A and B solutions were mixed quickly and then continued to react under ultrasonic treatment. After 5 min, the as-derived gelation as shown in Figure S1a in the Supporting Information were washed with DI water by vacuum filtration several times and dried at 50 °C for 24 h. Moreover, various samples were also prepared with different ratio of CeO_2 NPs and aniline to study the structures and morphologies of CeO_2 NP@PANI. The weight feed ratio of CeO_2 to aniline was varied as 0.5, 2, 4, and 6, and the resulting composites were denoted as CPA0.5, CPA2, CPA4, and CPA6, respectively. For reference, pure PANI hydrogel-doped by phytic acid was also prepared as control.

2.4. Characterization. The as-prepared nanocomposites were studied by field emission scanning electron microscopy (CARL ZEISS Supra55) and transmission electron microscopy (JEOL2100). X-ray diffraction (XRD) patterns were recorded using Philips Xpert PRO system with CuKα radiation from the range of 20−80°. Fourier transform infrared (FTIR) spectrogram was tested by Thermo Nicolet 360. Thermogravimetric analysis (SDT_Q600), elemental analysis (Vario EL III), and X-ray spectroscopic (EDS) were also conducted to measure the PANI content. The electric properties were investigated through two probes by using semiconductor parameters analyzer (Agilent 4156C).

2.5. Sensor Performance Measurements. Sensor fabrication was similar to our previous report with proper modification (see the Supporting Information for details).[32] Gas sensing properties were tested by NS-4003 precision sensor analyzer (China Zhong-Ke Micronano IOT Ltd.) at room temperature. The response S of the sensor is defined as $S = R_0/R_g$, where R_0 is the initial resistance in air and R_g in the mixed gas of NH_3 and air.

3. RESULTS AND DISCUSSION

Panels a and b in Figure 1 showed typical SEM images of CeO_2 NPs and PANI hydrogel, respectively. The products of CeO_2 consisted of highly uniform particles with the size about 250 nm, whereas the CP hydrogel showed 3D dendritic interconnected nanofibers with diameters of approximately 150 nm. The roughness of CeO_2 surface observed in the TEM (Figure 2a) was ascribed to the annealing, which eliminated the byproducts of CeO_2. Moreover, SEM images also showed the walnutlike rough matrix morphology of PANI hydrogel on the surface of CeO_2 (Figure 1c, d), and the rough PANI shell on the surface had a large specific area and thus enhanced the contact area with gas, which enhanced the sensor property.[33] The conformality of CeO_2/PANI nanostructure of CPA4 was also confirmed by energy-dispersive X-ray spectroscopic (EDS) elemental maps of Ce, O, N, and C from the designated areas in Figure S1b, c in the Supporting Information.

The coating thicknesses of PANI on the CeO_2 NPs of CPA0.5, CPA2, CPA4, and CPA6 decreased from ca. 55 to 25 nm as shown in the TEM images of Figure 2. When the weight feed ratio of CeO_2 to aniline was 0.5, pure PANI marked by arrows can be clearly observed from Figure 2b and the average PANI coating was also thicker than the rest samples of CPA2, CPA4, and CPA6 in Figure 2c, e, f. Herein we demonstrated that modulating the ratio of organic and inorganic reagents could also accurately tune the coating thickness, which was different from traditional method of adjusting the polymerization time.[15,22]

The CeO_2 NPs, CeO_2 NP@PANI and pure PANI were characterized by XRD measurement as shown in Figure 2d. Red line in the Figure exhibited sharp peaks corresponding to pure cubic CeO_2 with cell constants of a = 5.41 Å (JCPDS No.65−5925). A broad peak centered around 25° (110 face of PANI) could be observed, while there was no conspicuous additional peak of crystalline order or chain arrangement from the comparison of CeO_2 NP and CPA4, which suggested that the crystal structure of CeO_2 was not affected by PANI but the CeO_2 particle hindered the PANI molecular chains organization, indicating the amorphous nature of PANI shell.[34,35]

The PANI contents and thermal stability of samples were measured by TGA presented in Figure 3a. The weight loss (wt %) by decomposition of PANI at 1000 °C was decreased as the ratio of CeO_2 increased, manifesting the contents of PANI in CPA0.5 to CPA6 were ~41.6, 21.5, 14.7, and 10.4%, respectively. Element analyses also confirmed the contents of PANI by the presence of C, N, and H as shown in Table1.

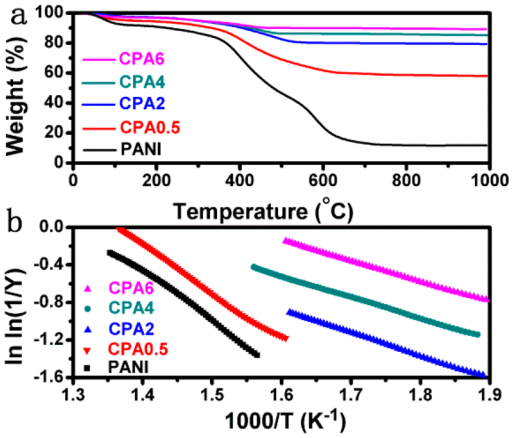

Figure 3. (a) TGA of PANI, CPA0.5, CPA2, CPA4 and CPA6, respectively. (b) Plots of ln ln(1/Y) vs 1000/T for the samples from PANI to CPA6.

Table 1. Weight Loss (%), Activation Energy of Thermo-oxidative Decomposition, and Element Analysis of C, N, and H for PANI, CPA0.5, CPA2, CPA4, and CPA6

samples	C (%)	N (%)	H (%)	Activation energy (kJ/mol)
PANI	43.56	7.854	3.823	43.81
CPA0.5	20.9	4.06	2.577	42.59
CPA2	7.793	1.552	1.155	20.45
CPA4	6.578	1.271	0.942	18.54
CPA6	5.271	0.968	0.849	18.20

The interaction between PANI and inorganic CeO_2 nanoparticles is correlated with the energy of activation (E_a) with the stage of thermo-oxidative decomposition beginning at around 400 °C.[36] E_a is described by a well-known Broido equation[37]

$$\ln\ln\left(\frac{1}{Y}\right) = \frac{-E_a}{RT} + C$$

where

$$Y = \frac{w_t - w_\infty}{w_0 - w_\infty}$$

w_0, w_∞, and w_s are the initial, final weight and weight at particular time, respectively. And Y is the fraction of the number of initial samples not yet decomposed. The plots of $\ln\ln(1/Y)$ versus $1000/T$ are approximate straight line as shown

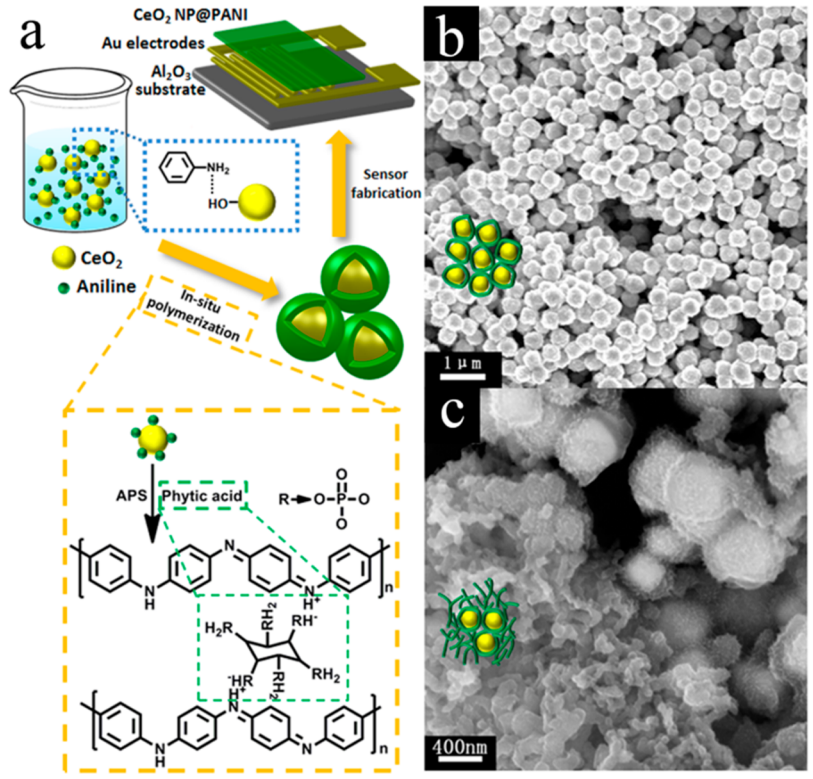

Figure 4. (a) Schematics of the fabrication of PANI hydrogel/CeO_2 core/shell gas sensors. (b) SEM image of CPA4 shows well-defined core/shell structure in proper CeO_2/aniline ratio. (c) SEM image of CPA0.5 exhibits three-dimensional network structure by existing homogeneously grown PANI hydrogel.

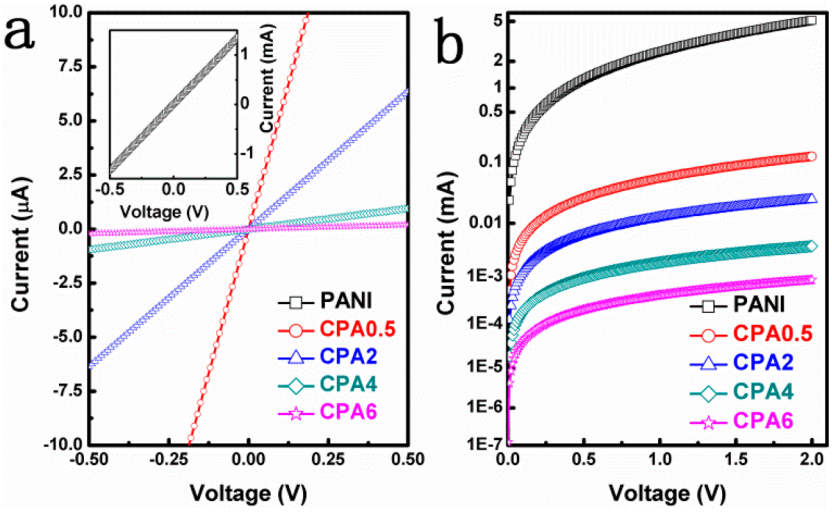

Figure 5. (a, b) *I*–*V* curves of different samples on a linear and semilog scale.

in Figure 3b. And the slopes of the plots are related to the activation energies whose values are listed in Table 1. The activation energies of pure PANI and CPA0.5 with low CeO_2 contents were higher than those of high CeO_2 to aniline ratios from Table 1. The decreased thermal stability of the nanocomposite proved by decreased activation energy may be caused by the interaction between cerium and nitrogen atom which is similar to the reported coordination of titanium and nitrogen.[36,38]The disappeared broad peak of PANI in CPA4 by XRD measurement also proved the coordination of Ce and N probably weakened the interchain interaction of PANI and certified the strong coordination between CeO_2 and PANI, which also suggested the formation of p–n junction. Herein, both TEM/SEM images and thermal stability analyses could prove the existence of p–n junction of nanohybrids.

In addition, FTIR measurement was conducted to have a deeper check of components in CPA4 and pure PANI as shown in Figure S2 in the Supporting Information, the characteristic peaks that corresponded to the stretching vibration of benzenoid ring and quinoid ring were located at 1384–1481 and 1570–1610 cm^{-1}, respectively, which indicated the chemical structure of phytic acid-doped PANI were emeraldine salt rather than solely leucoemeraldine or permigraniline form.[39,40]

Figure 4a illustrated the formation procedure of the PANI@CeO_2 core−shell structure. There is an electrostatic interaction between the anionic surface of CeO_2 and cationic aniline, so the columbic interaction binds them and also facilitates nucleation on the oxide surface.[41] Besides, the aniline monomer is highly soluble in the solution of CeO_2 nanoparticles as diagrammatizing in Figure 4a. After adding oxidation agent, heterocyclic polycation heterogeneously nucleates and accumulates on the exposed CeO_2 nanoparticles considering the solvophobic character of PANI.[42] When the ratio of CeO_2 to aniline was high, aniline was rapidly polymerized and cross-linked covering the surface of oxide forming a CP shell as shown in Figure 4b. Phytic acid molecule worked as gelator to grasp additional PANI chains by six strongly dissociated protons ($pK_a < 2$) of totally 12 replaceable ones, which was expected to improve the chemical stability of PANI@CeO_2 by the cross-linking effect compared with traditional organic−inorganic hybrids.[43,44] When the ratio of CeO_2 to aniline was 0.5, the additional aniline molecular aggregated homogeneously and also cross-linked by phytic acid, forming a combined structure of both zero-dimensional core−shell structure and dendritic-like three-dimensional network conducting polymer in Figure 4c.

Electrical properties of the sensors were also illustrated in Figure 5. Each device showed the linear increase of current with direct voltage in Figure 5a, indicating typical ohmic contacts between gold electrode and PANI shell of nanocomposite. These results were similar to the contact between pure PANI nanofibers and high work function metals such as Au and Pt reported by others.[45]The electricial properties in semilog scale were showed in Figure 5b. With decreasing thickness of PANI shell, the conductivity decreased exponentially, indicating the conduction channel mainly depended on the outside PANI layer.

Figure 6 displayed the typical response curves of CPA4, pure PANI and CeO_2 NPs upon exposure to 50 ppm of NH_3 at

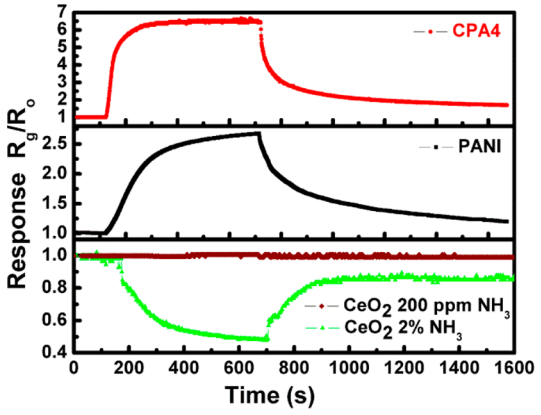

Figure 6. Typical response curves of CPA4, PANI ,and CeO_2 nanoparticles upon exposure to 50 ppm of NH_3 at room temperature. The bottom panel also exhibits the sensing response of CeO_2 to 2% at room temperature.

room temperature under a relative humidity of 58%. The CeO_2 exhibited no response at 50 ppm, whereas the resistance obviously decreased upon exposure to 2% (20 000 ppm) NH_3 as shown in Figure 6, suggesting n-type behavior of CeO_2 NPs. Poor response of CeO_2 NPs might be explained by the limited modulation of the depletion layer by NH_3 owing to the surface states and oxygen adsorption without high-temperature operation or doping with noble metals.[46] And the distinct increasing resistance of CPA4 and pure PANI showed typical p-type characteristics. Meanwhile CPA4 showed apparent detection virtue of higher response magnitude of 6.5 and shorter detection time (57.6 s) compared with pure PANI (response of 2.6 and 290 s of response time). The improved sensing feature can be assigned to well-defined p-n heterojunction of CPA4 with core−shell structure as proved by the combination of thermal stability of TGA analyses and SEM and TEM images.

It is expected that the sensing performance of NH_3 gas sensor was affected by the PANI to CeO_2 ratio. Figure 7a showed the real time responses of CPA0.5 to CPA6 upon sequential exposure of 50, 75, and 100 ppm of NH_3. From comparison of the curves, the responses of CPA4 to NH_3 were higher than the rest samples. Further increasing the shell thickness would not improve the response, which was confirmed by the fact that the responses of both CPA0.5 and CPA2 were lower than CPA4. This might be explained that with increasing the PANI thickness the effect of p−n junction could be ignored. Furthermore, the diffusion rate of ammonia was lower in the thick PANI layer, which also decreased the response,[15] whereas the thinner PANI shell of the CeO_2 NP@PANI nanohybrid caused lower residual holes, also reducing the response. Additionally we noted that the response of pure PANI to NH_3 was lower than that of CeO_2 NP@PANI at any ratio, indicating coating PANI on CeO_2 NPs was favorable to enhance the response by taking full advantage of these two materials to express synergetic effect. Considering the base resistance could not totally recover as shown in Figure 7a, the response transients of the sensor based on CPA4 to 50, 75, and 100 ppm of NH_3 were expressed according to the surface reaction model obeying the Langmuir−Hinshelwood mechanism, which was suitable for irreversible gas sensing[47]

$$S(t) = S_\infty(1 - e^{-t/\tau_a})$$

where s_∞ is the max response after the sensor has saturated, τ_a is the characteristic response time related to the initial gas concentration and surface reaction rate constant. The fitted curves showed comparative consistency with the experimental results in Figure 7b. And the fitted τ_a (11.89, 18.64, and 23.02) with increasing NH_3 concentration was reduced disproportionately, which proved the irreversible type of CeO_2 NP@PANI based gas sensor.[48]

Figure 7c showed the response of CPA4 upon sequential exposure to NH_3 by different concentrations at room temperature. The results showed the sensor exhibited an excellent response behavior to a wide range of NH_3. The sensor based on CPA4 was also measured down to 2 ppm of NH_3 at room temperature as shown in the inset of Figure 7c. The obvious response of 1.211 to 2 ppm of NH_3 could be related to the rough PANI shell on the surface that owned large specific area and thus enhanced the contact area with gas, together with the existence of p−n junction by CeO_2 NPs and PANI shell. It should be emphasized that response time was much faster in higher concentration of NH_3 in Figure 7d agreeing with the reported result, which could be owing to the heterogeneousness in interaction between PANI and NH_3 when exposed to different contents of reagent gas.[27,49] Without other method such as illumination with IR lamp, the sensing device-based CeO_2@PANI showed a recovery period of ∼6 min because of the rough PANI shell, which provided large surface area for desorption process.

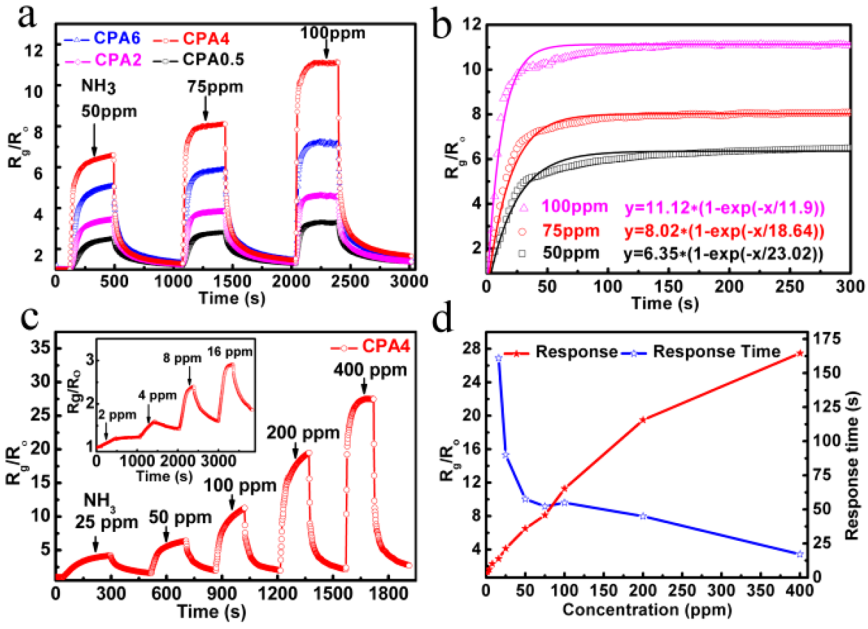

Figure 7. (a) Response curves of CPA0.5 to CPA6 upon sequential exposure of 50, 75, and 100 ppm of NH_3. (b) Fitted curves (solid lines) and experimental results (scattered points) of CPA4 to 50, 75, 100 ppm of NH_3. (c) Reversible and reproducible responses of CPA4 to different concentrations of NH_3. Inset is transient response of sequential exposure to 2, 4, 8, and 16 ppm of NH_3. (d) Response and response time of CPA4 to various NH_3 concentrations.

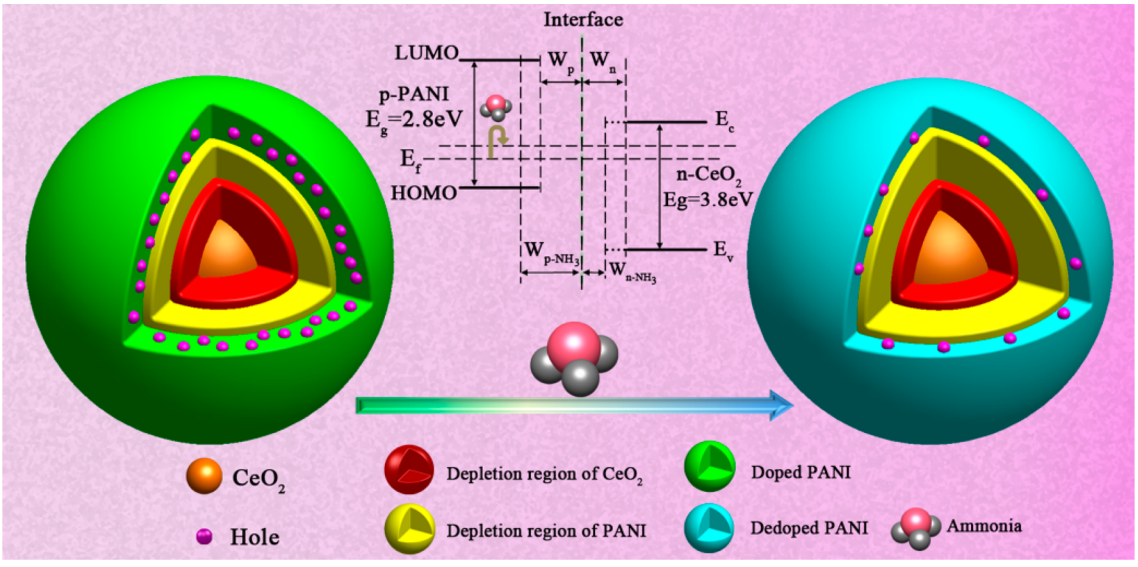

Figure 8. Schematic diagram showed the conducting pathway was mediated by synergic effect of CeO_2 core and PANI shell when exposed to NH_3 gas. The inset was schematic diagram of p−n junction in equilibrium state.

Additionally, we tested the sensor response of CeO_2 NP@PANI to 50 ppm of NH_3 at different temperatures as shown in Figure S3 in the Supporting Information. With the increase in temperature, the response clearly decreased and the color of CPA4 changed from green to black (the insets in Figure S3 in the Supporting Information). Moreover, the resistance of sensor increased and the sensor lost its sensing ability when heated up to 523 K, which was agreed with the thermal stability measured by TGA. These results indicated that the sensor got better sensing characteristics without additional heating and could work at room temperature.

The gas sensor-based on CeO_2 NP@PANI demonstrated much high response at room temperature, which could be attributed to the effect of well-known p-n heterojunctions. One possible mechanism is the reduction of the activation energy and enthalpy of physical adsorption by p-n heterojunction for NH_3 with good electron-donating characteristics.[10,49,50] To further understand the synergic effect of the heterojunctions, the modulation model of the conducting region by p−n junctions could probably explain the enhancement of the response of NH_3 gas sensor.[28] The schematic energy diagram of the heterojunction between CeO_2 and PANI was shown in the inset of Figure 8. The space charge region (the depletion layer) is naturally formed at the equilibrium condition. When exposed to electron-donating NH_3, the concentration of holes in the positively charged PANI backbone was reduced due to the well-known dedoping reaction (Scheme 1). In this case, NH_3 leaded to the conversion of PANI from emeraldine salt (ES) to

Scheme 1. Reaction Mechanism of PANI to NH_3

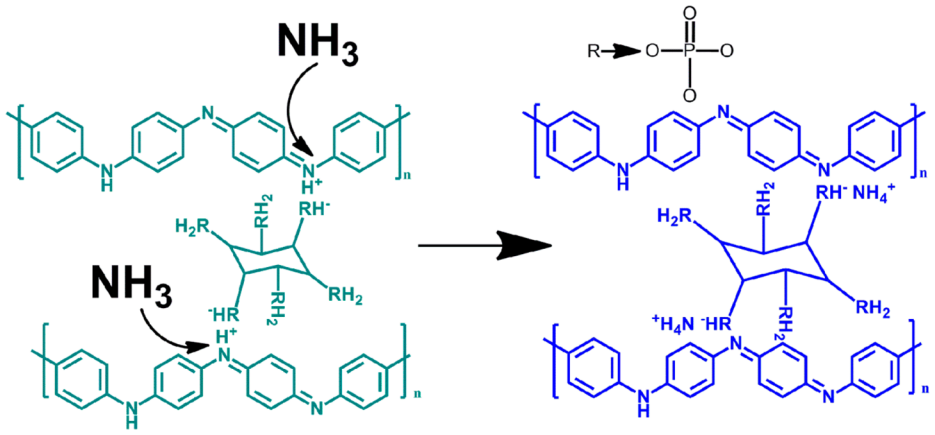

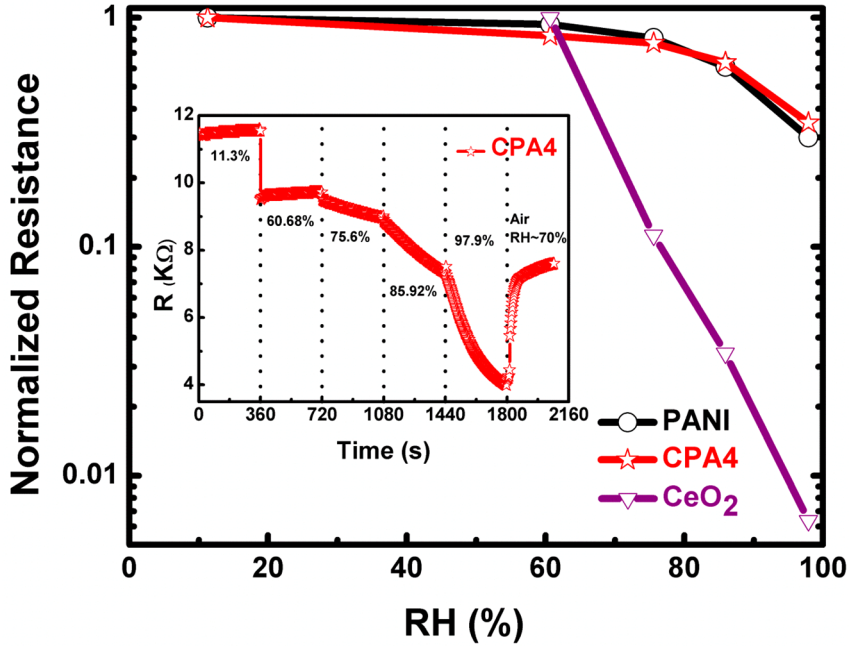

Figure 9. Response profiles of CeO_2, PANI, and CPA4 show the changes of resistances in different RH. Inset is real time response of CPA4 in different RH.

emeraldine base (EB), which increased the resistance of the outer PANI. Additionally, with regard to the total number of holes was reduced, there would be an increase of the depletion layer in the PANI sheath (inset of Figure 8 from W_p to $W_{p\text{-}NH3}$). Then the conducting pathway was reduced, as shown in Figure 9 from the thicker green shell (ES form of PANI) to thinner blue sheath (EB form of PANI). Considering the intrinsic high resistance of CeO_2, the decreased conducting region of PANI increased the resistance of whole structure further.

It had been demonstrated that humidity had a great effect on the performance of PANI and CeO_2-based sensors.[10,31] Additionally, a "reversed behavior" could happen to nanostructured PANI whose electrical resistance would increase at high relative humidity (RH) (>50%) due to distortion during polymer swelling.[40] So we investigated the relationship between relative humidity and the resistances of PANI, CPA4, and CeO_2 NPs, particularly in high RH range. Response profile in Figure 9 showed that the resistances of all samples would decrease with increasing RH. CeO_2 with high charge density in the surface exhibited an exponential reduction in high RH which followed the ion-type conductivity as the sensing mechanism.[51] Meanwhile, pure PANI also exhibited decreasing resistance when exposed to high relative humidity because of the well-known "proton effect".[24,40,52] In the chemical mechanism, when water molecules are absorbed on the PANI chains, proton from water sources can either dope PANI further or conduct charge themselves through absorbed water by the following reaction[53]

$$NH_2^+ + H_2O \leftrightarrow NH + H_3O^+$$

The response of CPA4 (inset of Figure 9) was much akin to the pure PANI rather than CeO_2 NPs. It is crucial to stress that the cross-linked PANI by phytic acid formed interconnected structure, which could acclimatize itself to the swelling from water absorption and did not show any resistance increasing by distortion of PANI chains in high RH.

Gas sensors for practical applications need good reproducibility besides high sensitivity and fast response. Figure 10a showed the response of CPA4 tested at a fixed concentration of 50 and 25 ppm through four cycles. The baseline had a drift of 13% from the initial state after first exposure to NH_3 similar to

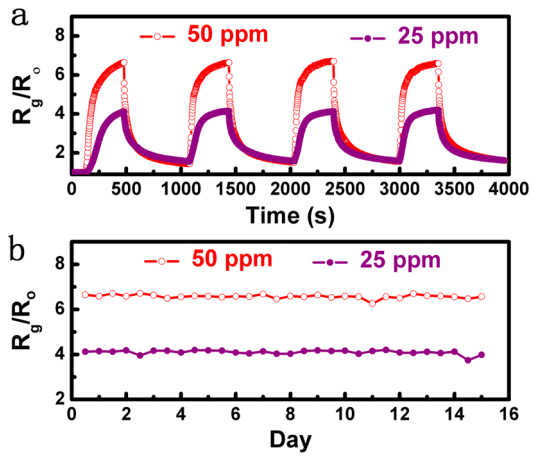

Figure 10. (a) Response of CPA4 tested at a fixed concentration of 50 and 25 ppm of NH_3 through four cycles. (b) Gas sensor of CPA4 stored unencapsulated at room temperature maintained its sensing characteristic after 30 cycles in 15 days.

other reports, which could be attributed to the relative irreversible reactions between strong acidic phytic acid and ammonia.[54] And the gelator phytic acid with nonvolatile nature worked as a cross-linker to weaken the impact of environment by increasing the mechanical strength and chemical stability of sensor, which could result in enhanced long-term stability. To verify the supposition, we stored the sensors of CPA4 unencapsulated at room temperature, and it still maintained its sensing characteristic (response of ca. 6.5 to 50 ppm of NH_3) after 30 cycles in 15 days which exhibited excellent stability as shown in Figure 10b. Thus, we believe the chemical cross-linking between polymer chains is a helpful method to both solve the intrinsic instability of the sensors based on CP and get a high response (as compared in Table 2).

Figure S4 in the Supporting Information showed the response in histogram of CPA4 to several gases at 50 ppm testing the selectivity of the sensor. Among the tested gases, nearly no response was observed when exposed to nitrogen dioxide, ethanol, and acetone, whereas the sensor upon exposure to hydrothion exhibited slight decrease of resistance which was much lower compared with the change of NH_3. The combined doping/dedoping process with regulating conducting pathway by p−n heterojunction may be assigned to the excellent selectivity. Sensor based on this hybridization of inorganic MOX and organic CP shows the potential application for selective detection of NH_3 at room temperature.

4. CONCLUSIONS

In summary, the CeO_2@PANI nanohybrids have been fabricated by in situ polymerization of aniline in the presence of CeO_2 NPs. Compared with other samples, the response of CPA4 to 50 ppm ammonia at room temperature was 6.5 and the response time was also decreased to 57.6 s, which exhibited higher performance. Improved sensing characteristics were related to the p−n heterojuction formed by CeO_2 NPs core and PANI shell. The formation of p−n junction was confirmed by decreased thermal stability of CeO_2@PANI nanohybrids. In particular, the PANI hydrogel sheath cross-linked by phytic acid displayed good stability to environmental atmosphere by its self-adjusting effect, which showed combined excellent sensitivity with superior long-term stability in contrast to the traditional conception of polymer-based ammonia sensor. Further effort could be made to decrease the baseline drift and moreover reducing the humidity effect to design functional gas sensors.

■ ASSOCIATED CONTENT

Supporting Information

Sensor fabrication and sensing measurements details, the photograph of the PANI hydrogel, EDS images, and FTIR spectra of materials and selectivity of CPA4. This material is available free of charge via the Internet at http://pubs.acs.org.

■ AUTHOR INFORMATION

Corresponding Author

*E-mail: thwang@xmu.edu.cn. Fax: +86-0592-2187196. Tel: +86-0592-2183063.

Notes

The authors declare no competing financial interest.

■ ACKNOWLEDGMENTS

This research was partly supported by the National Basic Research Program of China (Grant 2007CB310500).

■ REFERENCES

(1) Niihara, K.; Hirai, T. Chemical Vapour-Deposited Silicon Nitride. *J. Mater. Sci.* **1976**, *11*, 593−603.

(2) Timmer, B.; Olthuis, W.; Berg, A. Ammonia Sensors and Their Applications—A Review. *Sens. Actuators, B* **2005**, *107*, 666−677.

(3) Xu, C. N.; Miura, N.; Ishida, Y.; Matsuda, K.; Yamazoe, N. Selective Detection of NH_3 Over NO in Combustion Exhausts by Using Au and MoO_3 Doubly Promoted WO_3 Element. *Sens. Actuators, B* **2000**, *65*, 163−165.

(4) Wang, J.; Wei, L. M.; Zhang, L. Y.; Zhang, J.; Wei, H.; Jiang, C. H.; Zhang, Y. F. Zinc-doped Nickel Oxide Dendritic Crystals with Fast

Table 2. Sensing Performance of MOX, MOX-PANI, and RGO−PANI Hybrid Sensors for the Detection of NH_3 Gas[a]

materials	T (°C)	surface morphology	response	t (s)	stability	ref
CeO_2@PANI	RT	core−shell	6.5 (50 ppm)	57.6	response stayed the same after 15 days (30 cycles)	
5 wt % MoO_3 −WO_3	450		11 (5 ppm)	~60		3
Zn-doped NiO	RT	christmas-tree-like structure	0.4 (50 ppm)	5		4
In_2O_3	300	nanorods	18 (80 ppm)	~50		5
RGO−PANI hybrids	RT	RGO decorated by PANI NPs	1.59 (50 ppm)	500		20
graphene/PANI	RT	nanosheet/nanofiber	11.33 (100 ppm)	50	response decreased to ca. 57% after 5 days and ca. 48.5% after 9 days	9
PANI/TiO_2	RT	nanofiber	5.55 (117 ppm)	5	response decreased to ca. 58% after 4 days	10

[a] T is the working temperature; t is the response time; RT means room temperature.

Response and Self-recovery for Ammonia Detection at Room Temperature. *J. Mater. Chem.* **2012**, *22*, 20038−20047.
(5) Rout, C. S.; Hegde, M.; Govindaraj, A.; Rao, C. N. R. Ammonia Sensors Based on Metal Oxide Nanostructures. *Nanotechnology* **2007**, 20550401−20550409.
(6) Wang, S. R.; Kang, Y. F.; Wang, L. W.; Zhang, H. X.; Wang, Y. H.; Wang, Y. Organic/Inorganic Hybrid Sensors: A Review. *Sens. Actuators, B* **2013**, *182*, 467−481.
(7) Kukla, A. L.; Shirshov, Y. M.; Piletsky, S. A. Ammonia Sensors Based on Sensitive Polyaniline Films. *Sens. Actuators, B* **1996**, *37*, 135−140.
(8) Stamenov, P.; Madathil, R.; Coey, J. M. D. Dynamic Response of Ammonia Sensors Constructed from Polyaniline Nanofiber Films with Varying Morphology. *Sens. Actuators, B* **2012**, *161*, 989−999.
(9) Wu, Z.; Chen, X.; Zhu, S.; Zhou, Z.; Yao, Y.; Quan, W.; Liu, B. Enhanced Sensitivity of Ammonia Sensor Using Graphene/Polyaniline Nanocomposite. *Sens. Actuators, B* **2013**, 485−493.
(10) Tai, H.; Jiang, Y.; Xie, G.; Yu, J.; Chen, X. Fabrication and Gas Sensitivity of Polyaniline−Titanium Dioxide Nanocomposite Thin Film. *Sens. Actuators, B* **2007**, *125*, 644−650.
(11) Pan, L. J.; Yu, G.; Zhai, D.; Lee, H. R.; Zhao, W.; Liu, N.; Wang, H.; Tee, B. C. K.; Shi, Y.; Cui, Y. Hierarchical Nanostructured Conducting Polymer Hydrogel with High Electrochemical Activity. *Proc. Natl. Acad. Sci. U.S.A.* **2012**, *109*, 9287−9292.
(12) Bai, H.; Sheng, K.; Zhang, P.; Li, C.; Shi, G. Graphene Oxide/Conducting Polymer Composite Hydrogels. *J. Mater. Chem.* **2011**, *21*, 18653−18658.
(13) Zhai, D. Y.; Liu, B. R.; Shi, Y.; Pan, L. J.; Wang, Y. Q.; Li, W. B.; Zhang, R.; Yu, G. H. Highly Sensitive Glucose Sensor Based on Pt Nanoparticle/Polyaniline Hydrogel Heterostructures. *ACS Nano* **2013**, *7*, 3540.
(14) Heller, A. Electron-Conducting Redox Hydrogels: Design, Characteristics and Synthesis. *Curr. Opin. Chem. Biol.* **2006**, *10*, 664−672.
(15) Jiang, T. T.; Wang, Z. J.; Li, Z. Y.; Wang, W.; Xu, X. T.; Liu, X. C.; Wang, J. F.; Wang, C. Synergic Effect within n-Type Inorganic−p-Type Organic Nano-hybrids in Gas Sensors. *J. Mater. Chem. C* **2013**, *1*, 3017−3025.
(16) Ding, M.; Tang, Y.; Gou, P.; Reber, M. J.; Star, A. Chemical Sensing with Polyaniline Coated Single-Walled Carbon Nanotubes. *Adv. Mater.* **2011**, *23*, 536−540.
(17) Liao, Y.; Zhang, C.; Zhang, Y.; Strong, V.; Tang, J.; Li, X.-G.; Kalantar-zadeh, K.; Hoek, E. M. V.; Wang, K. L.; Kaner, R. B. Carbon Nanotube/Polyaniline Composite Nanofibers: Facile Synthesis and Chemosensors. *Nano Lett.* **2011**, *11*, 954−959.
(18) Yang, L. C.; Wang, S. N.; Mao, J. J.; Deng, J. W.; Gao, Q. S.; Tang, Y.; Schmidt, O. G. Hierarchical MoS_2 /Polyaniline Nanowires with Excellent Electrochemical Performance for Lithium-Ion Batteries. *Adv. Mater.* **2013**, *25*, 1180−1184.
(19) Wang, H. L.; Hao, Q. L.; Yang, X. J.; Lu, L. D.; Wang, X. Effect of Graphene Oxide on the Properties of Its Composite with Polyaniline. *ACS Appl. Mater. Interfaces* **2010**, *2*, 821−828.
(20) Huang, X. L.; Hu, N. T.; Gao, R. G.; Yu, Y.; Wang, Y. Y.; Yang, Z.; Kong, E. S.; Wei, H.; Zhang, Y. F. Reduced Graphene Oxide−Polyaniline Hybrid: Preparation, Characterization and Its Applications for Ammonia Gas Sensing. *J. Mater. Chem.* **2012**, *22*, 22488−22495.
(21) Taccola, S.; Greco, F.; Zucca, A.; Innocenti, C.; De Julián Fernández, C.; Campo, G.; Mattoli, V. Characterization of Free-Standing PEDOT:PSS/Iron Oxide Nanoparticle Composite Thin Films and Application As Conformable Humidity Sensors. *ACS Appl. Mater. Interfaces* **2013**, *5*, 6324−6332.
(22) Chen, S.; Sun, G. High Sensitivity Ammonia Sensor Using a Hierarchical Polyaniline/Poly(ethylene-co-glycidyl methacrylate) Nanofibrous Composite Membrane. *ACS Appl. Mater. Interfaces* **2013**, *5*, 6473−6477.
(23) Athawale, A. A.; Bhagwat, S. V.; Katre, P. P. Nanocomposite of Pd−Polyaniline as A Selective Methanol Sensor. *Sens. Actuators, B* **2006**, *114*, 263−267.
(24) Diggikar, R. S.; Kulkarni, M. V.; Kale, G. M.; Kale, B. B. Formation of Multifunctional Nanocomposites with Ultrathin Layers of Polyaniline (PANI) on Silver Vanadium Oxide (SVO) Nanospheres by In Situ Polymerization. *J. Mater. Chem. A* **2013**, *1*, 3992−4001.
(25) Lin, Q. Q.; Li, Y.; Yang, M. J. Gas Sensing Properties of Layer-by-layer Self-assembled Ultrathin Film of Polyaniline/Titanium Dioxide. *Synth. Met.* **2012**, *162*, 2242−2249.
(26) Savage, N. O. Gas Sensing Composites of Metal Oxides with Vapor-Deposited Polypyrrole. *Sens. Actuators, B* **2009**, *143*, 6−11.
(27) Dhawale, D. S.; Salunkhe, R. R.; Patil, U. M.; Gurav, K. V.; More, A. M.; Lokhande, C. D. Room Temperature Liquefied Petroleum gas (LPG) Sensor Based on p-Polyaniline/n-TiO_2 Heterojunction. *Sens. Actuators, B* **2008**, *134*, 988−992.
(28) Ho, T. A.; Jun, T. S.; Kim, Y. S. Material and NH_3-Sensing Properties of Polypyrrole-Coated Tungsten Oxide Nanofibers. *Sens. Actuators, B* **2013**, *185*, 523−529.
(29) Lee, J. S.; Shin, D. H.; Jun, J.; Jang, J. Multidimensional Polypyrrole/Iron Oxyhydroxide Hybrid Nanoparticles for Chemical Nerve Gas Agent Sensing Application. *ACS Nano* **2013**, *7*, 10139−10147.
(30) Wu, H.; Yu, G.; Pan, L.; Liu, N.; McDowell, M. T.; Bao, Z.; Cui, Y. Stable Li-ion Battery Anodes by In-situ Polymerization of Conducting Hydrogel to Conformally Coat Silicon Nanoparticles. *Nat. Commun.* **2013**, *4*, 1943.
(31) Sen, T.; Shimpi, N. G.; Mishra, S.; Sharma, R. Polyaniline/γ-Fe_2O_3 Nanocomposite for Room Temperature LPG Sensing. *Sens. Actuators, B* **2014**, *190*, 120−126.
(32) Liu, B.; Cai, D. P.; Liu, Y.; Li, H.; Weng, C.; Zeng, G. S.; Li, Q. H.; Wang, T. H. High-Performance room-Temperature Hydrogen Sensors Based on Combined Effects of Pd Decoration and Schottky Barriers. *Nanoscale* **2013**, *5*, 2505.
(33) Wang, D.; Chu, X.; Gong, M. Single-Crystalline $LaFeO_3$ Nanotubes with Rough Tube Walls: Synthesis and Gas-Sensing Properties. *Nanotechnology* **2006**, *17*, 5501−5505.
(34) Xia, H. S.; Wang, Q. Ultrasonic Irradiation: A Novel Approach to Prepare Conductive Polyaniline/Nanocrystalline Titanium Oxide Composites. *Chem. Mater.* **2002**, *14*, 2158−2165.
(35) He, Y. J. Synthesis of Polyaniline/Nano-CeO_2 Composite Microspheres via A Solid-Stabilized Emulsion Route. *Mater. Chem. Phys.* **2005**, *92*, 134−137.
(36) Ansari, M. O.; Mohammad, F. Thermal Stability, Electrical Conductivity and Ammonia Sensing Studies on p-Toluenesulfonic Acid Doped Polyaniline:Titanium Dioxide (pTSA/Pani:TiO_2) Nanocomposites. *Sens. Actuators, B* **2011**, *157*, 122−129.
(37) Rangraj, A.; Vangani, V.; Rakshit, A. K. Synthesis and Characterization of Some Water Soluble Polymers. *J. Appl. Polym. Sci.* **1997**, *66*, 45−56.
(38) Zheng, J. B.; Li, G.; Ma, X. F.; Wang, Y. M.; Wu, G.; Cheng, Y. N. Polyaniline−TiO_2 Nano-composite-based Trimethylamine QCM Sensor and Its Thermal Behavior Studies. *Sens. Actuators, B* **2008**, *133*, 374−380.
(39) Wang, Y. F.; Yang, X. W.; Qiu, L.; Li, D. Revisiting the Capacitance of Polyaniline by Using Graphene Hydrogel Films as A Substrate: the Importance of Nano-architecturing. *Energy Environ. Sci.* **2013**, *6*, 477−481.
(40) Zeng, F. W.; Liu, X. X.; Diamond, D.; Lau, K. T. Humidity Sensors Based on Polyaniline Nanofibres. *Sens. Actuators, B* **2010**, 530−534.
(41) Xia, X.; Chao, D.; Qi, X.; Xiong, Q.; Zhang, Y.; Tu, J.; Zhang, H.; Fan, H. J. Controllable Growth of Conducting Polymers Shell for Constructing High-Quality Organic/Inorganic Core/Shell Nanostructures and Their Optical-Electrochemical Properties. *Nano Lett.* **2013**, *13*, 4562−4568.
(42) Li, D.; Huang, J. X.; Kaner, R. B. Polyaniline Nanofibers: A Unique Polymer Nanostructure for Versatile Applications. *Acc. Chem. Res.* **2008**, *42*, 135−145.
(43) Rounds, M. A.; Nielsen, S. S. Anion-Exchange High-Performance Liquid Chromatography with Post-Column Detection for the

Analysis of Phytic Acid and Other Inositol Phosphates. *J. Chromatogr. A* **1993**, *653*, 148−152.
(44) Li, J.; Zhu, L. H.; Wu, Y. H.; Harima, Y.; Zhang, A. Q.; Tang, H. Q. Hybrid Composites of Conductive Polyaniline and Nanocrystalline Titanium Oxide Prepared via Self-assembling and Graft Polymerization. *Polymer* **2006**, *47*, 7361−7367.
(45) Fowler, J. D.; Virji, S.; Kaner, R. B.; Weiller, B. H. Hydrogen Detection by Polyaniline Nanofibers on Gold and Platinum Electrodes. *J. Phys. Chem. C* **2009**, *113*, 6444−6449.
(46) Liao, L.; Mai, H. X.; Yuan, Q.; Lu, H. B.; Li, J. C.; Liu, C.; Yan, C. H.; Shen, Z. X.; Yu, T. Single CeO_2 Nanowire Gas Sensor Supported with Pt Nanocrystals: Gas Sensitivity, Surface Bond States, and Chemical Mechanism. *J. Phys. Chem. C* **2008**, *112*, 9061−9065.
(47) Bai, S. L.; Guo, T.; Zhao, Y. B.; Luo, R. X.; Li, D. Q.; Chen, A. F.; Liu, C. C. Mechanism Enhancing Gas Sensing and First-Principle Calculations of Al-doped ZnO Nanostructures. *J. Mater. Chem. A* **2013**, *1*, 11335.
(48) Lee, C. Y.; Strano, M. S. Understanding the Dynamics of Signal Transduction for Adsorption of Gases and Vapors on Carbon Nanotube Sensors. *Langmuir* **2005**, *21*, 5192−5196.
(49) Geng, L. N.; Zhao, Y. Q.; Huang, X. L.; Wang, S. R.; Zhang, S. M.; Wu, S. H. Characterization and Gas Sensitivity Study of Polyaniline/SnO_2 Hybrid Material Prepared by Hydrothermal Route. *Sens. Actuators, B* **2007**, *120*, 568−572.
(50) Benjamin, P. J.; Phillip, E.; Richard, J. E.; Colin, L. H.; Norman, M. R. Novel Composite Organic-Inorganic Semiconductor Sensors for the Quantitative Detection of Target Organic Vapour. *J. Mater. Chem.* **1996**, *6*, 289−294.
(51) Fu, X. Q.; Wang, C.; Yu, H. C.; Wang, Y. G.; Wang, T. H. Fast Humidity Sensors Based on CeO_2 Nanowires. *Nanotechnology* **2007**, *18*, 145503−145506.
(52) Parvatikar, N.; Jain, S.; Khasim, S.; Revansiddappa, M.; Bhoraskar, S. V.; Prasad, M. V. N. A. Electrical and Humidity Sensing Properties of Polyaniline/WO_3 Composites. *Sens. Actuators, B* **2006**, *114*, 599−603.
(53) Li, Y.; Ying, B. Y.; Hong, L. J.; Yang, M. J. Water-soluble Polyaniline and Its Composite with Poly(vinyl alcohol) for Humidity Sensing. *Synth. Met.* **2010**, *160*, 455−461.
(54) Matsuguchi, M.; Asahi, T. Properties and Stability of Polyaniline Nanofiber Ammonia Sensors Fabricated by Novel On-Substrate Method. *Sens. Actuators, B* **2011**, *160*, 999−1004.